Engineering with Computers (2021) 37:2823–2836
https://doi.org/10.1007/s00366-020-00976-2

ORIGINAL ARTICLE

Buckling and post-buckling behaviors of higher order carbon nanotubes using energy-equivalent model

N. Mohamed[1] · S. A. Mohamed[1] · M. A. Eltaher[2,3]

Received: 20 November 2018 / Accepted: 31 January 2020 / Published online: 15 February 2020

Abstract
This paper aims to investigate the size scale effect on the buckling and post-buckling of single-walled carbon nanotube (SWCNT) rested on nonlinear elastic foundations using energy-equivalent model (EEM). CNTs are modelled as a beam with higher order shear deformation to consider a shear effect and eliminate the shear correction factor, which appeared in Timoshenko and missed in Euler–Bernoulli beam theories. Energy-equivalent model is proposed to bridge the chemical energy between atoms with mechanical strain energy of beam structure. Therefore, Young's and shear moduli and Poisson's ratio for zigzag (*n,* 0), and armchair (*n, n*) carbon nanotubes (CNTs) are presented as functions of orientation and force constants. Conservation energy principle is exploited to derive governing equations of motion in terms of primary displacement variable. The differential–integral quadrature method (DIQM) is exploited to discretize the problem in spatial domain and transformed the integro-differential equilibrium equations to algebraic equations. The static problem is solved for critical buckling loads and the post-buckling deformation as a function of applied axial load, CNT length, orientations and elastic foundation parameters. Numerical results show that effects of chirality angle, boundary conditions, tube length and elastic foundation constants on buckling and post-buckling behaviors of armchair and zigzag CNTs are significant. This model is helpful especially in mechanical design of NEMS manufactured from CNTs.

Keywords Differential–integral quadrature method · Carbon nanotube · Energy-equivalent model · Static post-buckling instability · Nonlinear integro-differential equation

1 Introduction

Since 1991, carbon nanotubes (CNTs), discovered by Iijima, have received widespread interest of researchers due to their extraordinary mechanical, thermal, physical and electrical properties. CNTs are considered the strongest and most resilient material known until now, [32]. In general, geometrical and mechanical properties of CNTs are controlled by two parameters [12], which are the orientation of the chiral angle and the carbon diameter. The chiral vector and tube radius (R) of CNTs can be portrayed by

$$\vec{C}_h = n\vec{a}_1 + m\vec{a}_2, \tag{1.a}$$

$$R = l_0\sqrt{3\left(n^2 + m^2 + n^*m\right)}/2\pi. \tag{1.b}$$

In which the unit vectors are $\vec{a}_1$ and $\vec{a}_2$, and (n, m) is integer pair that specifies the structure orientation of CNTs [i.e.: zigzag at $(n, 0)$, armchair at (n, n), and chiral orientation at (n, m) for $m \neq n$ or 0] as presented in Fig. 1. The C–C bond length here is $l_0 = 0.142$ nm. Zigzag and armchair nanotubes radii are calculated by $R = \frac{\sqrt{3}nl_0}{2\pi}$ and by $R = \frac{3nl_0}{2\pi}$, respectively.

Nasdala et al. [34] illustrated that the standard truss and beam elements can be represented atomic interactions accurately. Energy-equivalent model, resulting from the foundation of molecular and continuum mechanics, considers the mechanical properties of CNTs (i.e.; Young's modulus, shear

✉ M. A. Eltaher
meltaher@kau.edu.sa; mohaeltaher@gmail.com

1 Department of Engineering Mathematics, Faculty of Engineering, Zagazig University, Zagazig, Egypt

2 Mechanical Engineering Department, Faculty of Engineering, King Abdulaziz University, Jeddah, Saudi Arabia

3 Mechanical Design and Production Department, Faculty of Engineering, Zagazig University, Zagazig, Egypt

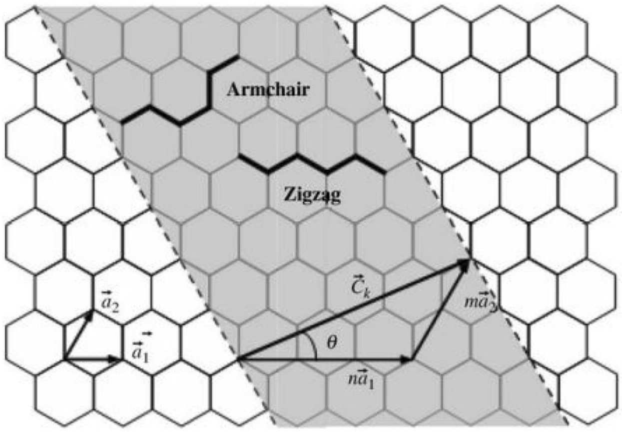

Fig. 1 Schematic diagram of the chiral vector and the choral angle of CNTs, [42]

modulus, and Poisson's ratio) as a material size dependent by many researchers. Leung et al. [27] proposed a combined model of molecular and continuum mechanics to investigate mechanical properties of zigzag SWCNTs. Wu et al. [42] derived the equivalent Young's and shear moduli for both armchair and zigzag SWCNTs by combining molecular and continuum mechanics methods. In [30], derived an exact elastica solution for a clamped-simply (C-S) SWCNT by the elliptic integral technique. Aydogdu [1] studied, free vibration of simply supported (S–S) multi-walled carbon nanotubes (MWCNTs) using the higher order shear deformation beam theory (HOSDT). Mayoof and Hawwa [29] investigated nonlinear vibration of CNT with waviness along its axis based on classical continuum theory. Shodja and Delfani [38] and Shokrieh and Rafiee [39] presented analytical formulations to predict the elastic moduli of graphene sheets and CNTs using a linkage between lattice molecular structure and equivalent discrete frame structure. Joshi et al. [23] modeled the elastic behavior of CNT-reinforced composites using the multiscale representative volume element approach. Wang et al. [40, 41] studied the vibrations of S–S double-walled CNTs subjected to a moving harmonic load using nonlocal Euler and Timoshenko beam theories. Mohammadi et al. [33] investigated the static instability of an imperfect nonlocal Eringen nanobeam embedded in elastic foundation. Khater et al. [25] studied buckling behavior of curved nanowires including a surface energy under a thermal load. Ghadyani and Ochsner [19] presented an expression for the stiffness of SWCNTs as function of nanotube thickness. Eltaher and Agwa [9] presented a modified continuum energy-equivalent model to investigate the vibration of a pretension CNTs carrying a concentrated mass as a mass sensor.

Gholami et al. [20] analyzed the nonlinear resonant of imperfect HOSDT functionally graded carbon nanotube-reinforced composite beams subjected to a harmonic transverse load. Kordkheili et al. [26] employed nonlocal continuum theory of Eringen and Von Karman nonlinear strains to study a linear and nonlinear dynamics of SWCNTs conveying fluid with different boundary conditions. Mohamed et al. [31] exploited modified differential–integral quadrature method to analyze nonlinear free and forced vibrations of buckled curved beams resting on nonlinear elastic foundations. Maneshi et al. [28] presented closed-form expression for geometrically nonlinear large deformation of nanobeams subjected to end force. Emam et al. [18] investigated the post-buckling and free vibration response of geometrically imperfect multilayer nanobeams under pre-stress compressive load. Eltaher et al. [12] and Mohamed et al. [32] presented a novel numerical procedure to predict nonlinear buckling and post-buckling stability of imperfect clamped–clamped (C–C) SWCNTs surrounded by nonlinear elastic foundation using energy-equivalent model. Eltaher et al. [13] illustrated the influence of periodic (sine and cosine) and nonperiodic imperfection modes on buckling, post-buckling and dynamics of beam rested on nonlinear elastic foundations. Dehghan et al. [6] investigated the wave propagation of fluid-conveying magneto-electro-elastic nanotube incorporating fluid effect. Eltaher et al. [14] characterized Young's modulus and evaluated vibration and buckling behaviors of CNTs by equivalent-continuum mechanics approach. Karimiasl et al. [24] studied post-buckling behaviors of multiscale composite sandwich doubly curved piezoelectric shell with a flexible core by employing Homotopy Perturbation Method in hygrothermal environment. Eltaher et al. [15, 16] illustrated the effect of imperfections and vacancies on vibration and modal participation factor of CNTs using energy-equivalent model. Ebrahimi and Hosseini [7] presented the nonlinear vibration behavior and dynamic instability of Euler–Bernoulli nanobeams (EBT) under thermo-magneto-mechanical loads. Ebrahimi et al. [8] evaluated the damping forced harmonic vibration characteristics of magneto-electro-viscoelastic nanobeam embedded in viscoelastic foundation based on nonlocal strain gradient elasticity theory.

Based on both material and size dependency, many researchers studied buckling and vibration behaviors of CNTs. Baghdadi et al. [2] presented thermal effect on vibration of armchair and zigzag SWCNTs using nonlocal parabolic beam theory. Benguediab et al. [4] studied buckling properties of a zigzag double-walled CNT with both chirality and small-scale effects using Timoshenko beam. Semmah et al. (2015) presented the thermal buckling properties of a zigzag SWCNT based on the nonlocal Timoshenko beam and energy-equivalent model. Bedia et al. [3] studied analytically thermal buckling of armchair SWCNT embedded in an elastic medium. On the basis of the continuum mechanics and the single-elastic beam model, Besseghier et al. [5] investigated the nonlinear vibration of zigzag SWCNT embedded in elastic medium. Heshmati et al. [21] studied the vibrational behavior of CNT-reinforced composite beams and presented the effects the interface, waviness, agglomeration, orientation and length on the behavior of CNTs. Eltaher et al. [9] illustrated nonlinear static behavior of size-dependent and material-dependent nonlocal CNTs using nonlocal differential form of Eringen and energy-equivalent method. Eltaher et al. [11] presented a modified continuum model included energy-equivalent model and modified couple stress theory to investigate the vibration behavior of CNTs.

According to the best of the authors' knowledge and literature review, it can be concluded that no researchers have attempted to investigate buckling and post-buckling of higher order shear deformation CNTs by considering material size dependency. The present study intends to fill this gap in the literature by considering the energy-equivalent method along with HOSDT. This paper is organized as follows. Section 2 describes the mathematical formulation of the equivalent energy model for armchair and zigzag SWCNTs continuum. Main formulations and equilibrium governing equations of CNTs modeled by higher order shear deformation theory are presented. In Sect. 3, differential–integral quadrature method is presented and developed to solve equilibrium differential equations of material size-dependent carbon nanotube. Analytical solution and closed form for critical buckling load are presented through Sect. 4. Numerical results are presented and discussed in Sect. 5**.** Most findings and concluding remarks are summarized in Sect. 6.

2 Mathematical formulation

2.1 Chemical energies vs. mechanical energies

Comparing microscopic chemistry and the macroscopic mechanics energies, covalent bonds between carbon atoms can be represented by forces, which are functions of bond lengths and bond angles. Therefore, the force filed through bonding can be described by potential energies as [35]

$$\mathrm{PE} = \mathrm{PE}_L + \mathrm{PE}_\theta + \mathrm{PE}_T + \mathrm{PE}_\omega. \tag{2}$$

In which PE_L, PE_θ, PE_T, and PE_ω are bond stretching, angle variation, torsion and inversion (out of plane) energies. In 2D loading, the most significant energies are bending angle energies and bond stretching and the other energies can be neglected. Therefore, Eq. (2) can be simplified as [14-16]

$$\mathrm{PE} = \mathrm{PE}_L + \mathrm{PE}_\theta = \frac{1}{2}\sum_i K_i\left(dR_i\right)^2 + \frac{1}{2}\sum_j C_j\left(d\theta_j\right)^2, \tag{3}$$

where K_i is the stretching constant, dR_i is the elongation of the bond i, C_j is the angle variance constant, $d\theta_j$ is the variance of bond angle j. Young's modulus and Poisson's ratio for CNTs, for armchair and zigzag orientations, can be represented by Mohamed et al. [32]

$$E_a = \frac{4\sqrt{3}}{3}\frac{KC}{3Ct + 4Kl_0^2t\left(\lambda_{a1}^2 + 2\lambda_{a2}^2\right)}, \tag{4a}$$

$$\upsilon_a = \frac{\lambda_{a1}l_0^2K - C}{\lambda_{a1}l_0^2K + 3C}, \tag{4b}$$

$$E_z = \frac{4\sqrt{3}KC}{9Ct + 4Kl_0^2t\left(\lambda_{z1}^2 + 2\lambda_{z2}^2\right)}, \tag{4c}$$

$$\upsilon_z = \frac{\lambda_{z1}l_0^2K + \sqrt{3}C}{\lambda_{z1}l_0^2K - 3\sqrt{3}C}, \tag{4d}$$

where t is the thickness of a nanotube. Subscripts a and z represent armchair and zigzag, respectively. λ_1 and λ_2 are geometrical-dependent parameters, which can be evaluated by

$$\lambda_{a1}(n) = \frac{4 - \cos^2(\pi/2n)}{16 + 2\cos^2(\pi/2n)}, \tag{5a}$$

$$\lambda_{a2}(n) = \frac{-\sqrt{12 - 3\cos^2(\pi/2n)}\cos(\pi/2n)}{32 + 4\cos^2(\pi/2n)}, \tag{5b}$$

$$\lambda_{z1}(n) = \frac{-3\sqrt{4 - 3\cos^2(\pi/2n)}\cos(\pi/2n)}{8\sqrt{3} - 2\sqrt{3}\cos^2(\pi/2n)}, \tag{5c}$$

$$\lambda_{z2}(n) = \frac{12 - 9\cos^2(\pi/2n)}{16\sqrt{3} - 4\sqrt{3}\cos^2(\pi/2n)}, \tag{5d}$$

2.2 Geometrical formulation of CNTs

The displacement fields of the higher order shear deformation CNTs are represented by Aydogdu [1]

$$U_0(x,z,t) = u(x,t) - z\frac{\partial w(x,t)}{\partial x} + f(z)\phi(x,t), \tag{6a}$$

$$W_0(x,z,t) = w(x,t), \tag{6b}$$

where U_0, and W_0 are denoting the displacement components along the x- and z-directions, respectively. u and w represent middle surface displacement components along the x- and z-directions, respectively. ϕ is an unknown function that represents the effect of transverse shear strain on the beam middle surface, and $f(z)$ represents the shape function determining the distribution of the transverse shear strain and stress through the thickness, which can be described by Reddy [36]

$$f(z) = z\left(1 - \frac{4z^2}{3h^2}\right), \tag{7}$$

The nonzero strains of the CNTs associated with the displacement field given in Eq. (6) can be computed by

$$\varepsilon_{xx} = \frac{\partial U_0}{\partial x} + \frac{1}{2}\left(\frac{\partial W_0}{\partial x}\right)^2 = \varepsilon_x^{(0)} + z\varepsilon_x^{(1)} + f(z)\varepsilon_x^{(2)}, \tag{8a}$$

$$\gamma_{xz} = \frac{\partial U_0}{\partial z} + \frac{\partial W_0}{\partial x} = \frac{df}{dz}\gamma_{xz}^{(0)}, \tag{8b}$$

in which

$$\varepsilon_x^{(0)} = \frac{\partial u}{\partial x} + \frac{1}{2}\left(\frac{\partial w}{\partial x}\right)^2; \varepsilon_x^{(1)} = -\frac{\partial^2 w}{\partial x^2}; \varepsilon_x^{(2)} = \frac{\partial \phi}{\partial x}; \gamma_{xz}^{(0)} = \phi. \tag{9}$$

However, the stress constitutive equations may be written in the form

$$\sigma_{xx} = E\varepsilon_{xx} = E\left[\varepsilon_x^{(0)} + z\varepsilon_x^{(1)} + f(z)\varepsilon_x^{(2)}\right], \tag{10a}$$

$$\tau_{xz} = G\gamma_{xz} = \frac{E}{2(1+\mu)}\frac{\partial f}{\partial z}\gamma_{xz}^{(0)}. \tag{10b}$$

Hence, force and moment resultants may be written in the form

$$\begin{Bmatrix} N \\ M \\ P \end{Bmatrix} = \begin{bmatrix} A_1 & A_2 & A_3 \\ A_2 & A_4 & A_5 \\ A_3 & A_5 & A_6 \end{bmatrix} \begin{Bmatrix} \varepsilon_x^{(0)} \\ \varepsilon_x^{(1)} \\ \varepsilon_x^{(2)} \end{Bmatrix}, \tag{11a}$$

$$Q = A_7\gamma_{xz}^{(0)}, \tag{11b}$$

where A_j stiffness coefficients can be evaluated by

$$\left(A_1, A_2, A_3, A_4, A_5, A_6, A_7\right) = \int_A E(z)\left[1, z, f, z^2, zf, f^2, \left(\frac{df}{dz}\right)^2\right] dA. \tag{12}$$

Based on the conservation of energy, which states that variation of energy will be equal to zeros

$$\delta\Pi = \delta U + \delta V = 0, \tag{13}$$

where δU is the virtual strain energy, δV is the virtual work done by external forces, and

$$\begin{aligned} \delta U &= \frac{1}{2}\delta\left[\int_\Omega \left(\sigma_{xx}\varepsilon_{xx} + \tau_{xz}\gamma_{xz}\right) d\Omega\right] + \frac{1}{2}\bar{N}\,\delta\int_0^L \left(\frac{\partial w}{\partial x}\right)^2 dx \\ &= \int_0^L \left[N\delta\varepsilon_x^{(0)} + M\delta\varepsilon_x^{(1)} + P\delta\varepsilon_x^{(2)} + Q\delta\gamma_{xz}^{(0)}\right] dx \\ &\quad + \bar{N}\int_0^L \left(\frac{\partial w}{\partial x}\right)\left(\frac{\partial \delta w}{\partial x}\right) dx, \end{aligned} \tag{14a}$$

$$\delta V = -\delta\left[\int_\Gamma \left(\sigma_{xx}u + \tau_{xz}w\right) d\Gamma\right], \tag{14b}$$

where Ω and Γ denote domain and boundary of the beams. After performing variation operations, one can obtain

$$\delta u : \frac{\partial N}{\partial x} = 0, \tag{15a}$$

$$\delta w : \frac{\partial^2 M}{\partial x^2} + \frac{\partial}{\partial x}\left(N\frac{\partial w}{\partial x}\right) - \left(\bar{N} - \bar{k}_s\right)\frac{\partial^2 w}{\partial x^2} - \bar{k}_L w - \bar{k}_{NL} w^3 = 0, \tag{15b}$$

$$\delta\varphi : \frac{\partial P}{\partial x} - Q = 0, \tag{15c}$$

where the shear layer, linear and nonlinear Winkler stiffness are $\bar{k}_s$,$\bar{k}_L$ and $\bar{k}_{NL}$, respectively. The equilibrium equations can be represented in terms of displacements as

$$A_1\frac{d}{dx}\left[\frac{du}{dx} + \frac{1}{2}\left(\frac{dw}{dx}\right)^2\right] - A_2\frac{d^3 w}{dx^3} + A_3\left(\frac{d^2\phi}{dx^2}\right) = 0, \tag{16a}$$

$$\begin{aligned} &A_1\frac{d}{dx}\left\{\left[\frac{du}{dx} + \frac{1}{2}\left(\frac{dw}{dx}\right)^2\right]\frac{dw}{dx}\right\} + A_3\frac{d}{dx}\left[\frac{dw}{dx}\frac{d\phi}{dx}\right] \\ &\quad + A_2\frac{d^3 u}{dx^3} + A_5\left(\frac{d^3\phi}{dx^3}\right) - A_4\frac{d^4 w}{dx^4} - \left(\bar{N} - \bar{k}_s\right) \\ &\quad \frac{\partial^2 w}{\partial x^2} - \bar{k}_L w - \bar{k}_{NL} w^3 = 0, \end{aligned} \tag{16b}$$

$$A_3\frac{d}{dx}\left[\frac{du}{dx} + \frac{1}{2}\left(\frac{dw}{dx}\right)^2\right] - A_5\frac{d^3 w}{dx^3} + A_6\frac{d^2\phi}{dx^2} - A_7\phi = 0. \tag{16c}$$

To eliminate the axial displacement u in governing Eq. (16), Integrating Eq. (16a) with respect to the spatial coordinate x two times yields

$$u = -\frac{1}{2}\int_0^L \left(\frac{dw}{dx}\right)^2 dx + \frac{A_2}{A_1}\frac{dw}{dx} - \frac{A_3}{A_1}\phi + \frac{C_1}{A_1}x + C_2. \tag{17}$$

The boundary conditions for CNTs with immovable ends can be expressed as

$$u(0) = u(L) = 0. \tag{18}$$

After substituting and some manipulations, the following equations can be deduced:

$$\frac{du}{dx}+\frac{1}{2}\left(\frac{dw}{dx}\right)^2=\frac{1}{2L}\int_0^L\left(\frac{dw}{dx}\right)^2dx+\frac{A_2}{A_1}\frac{d^2w}{dx^2}-\frac{A_3}{A_1}\frac{d\phi}{dx}, \tag{19a}$$

$$\frac{d}{dx}\left[\frac{du}{dx}+\frac{1}{2}\left(\frac{dw}{dx}\right)^2\right]=\frac{A_2}{A_1}\frac{d^3w}{dx^3}-\frac{A_3}{A_1}\frac{d^2\phi}{dx^2}, \tag{19b}$$

$$\frac{d^3u}{dx^3}=-\frac{d}{dx}\left(\frac{dw}{dx}\frac{d^2w}{dx^2}\right)-\frac{A_3}{A_1}\frac{d^3\phi}{dx^3}+\frac{A_2}{A_1}\frac{d^4w}{dx^4}. \tag{19c}$$

Substituting Eq. (19) back into Eq. (16) yields

$$\left(\frac{A_2^2}{A_1}-A_4\right)\frac{d^4w}{dx^4}+\left[\frac{A_1}{2L}\int_0^L\left(\frac{dw}{dx}\right)^2dx-\bar{P}+\bar{k}_s\right]\frac{d^2w}{dx^2}-\bar{k}_Lw-\bar{k}_{NL}w^3+\left(A_5-\frac{A_2A_3}{A_1}\right)\frac{d^3\phi}{dx^3}=0, \tag{20a}$$

$$\left(A_6-\frac{A_3^2}{A_1}\right)\frac{d^2\phi}{dx^2}+\left(\frac{A_2A_3}{A_1}-A_5\right)\frac{d^3w}{dx^3}-A_7\phi=0. \tag{20b}$$

Computing the coefficients A_j and substituting into Eq. (20).

$$EI\frac{d^4w}{dx^4}+\left[\bar{P}-\bar{k}_s-\frac{EA}{2L}\int_0^L\left(\frac{dw}{dx}\right)^2dx\right]\frac{d^2w}{dx^2}+\bar{k}_Lw+\bar{k}_{NL}w^3-\frac{4}{5}EI\frac{d^3\phi}{dx^3}=0, \tag{21a}$$

$$\frac{68}{105}EI\frac{d^2\phi}{dx^2}-\frac{4}{5}EI\frac{d^3w}{dx^3}-\frac{8}{15}EA\phi=0, \tag{21b}$$

where the mass moment of inertia $I=\frac{\pi}{4}\left((R+t)^4-R^4\right)$ and the cross-sectional area $A=\pi\left((R+t)^2-R^2\right)$. Introducing the following nondimensional parameters

$$W=\frac{w}{L},X=\frac{x}{L},\Phi=\phi. \tag{22}$$

Equation (21) can be written in a dimensionless form as

$$\frac{d^4W}{dX^4}+\left[P-k_s-\frac{1}{2}\gamma_0\int_0^1\left(\frac{dW}{dX}\right)^2dx\right]\frac{d^2W}{dX^2}+k_LW+k_{NL}W^3-\gamma_1\frac{d^3\Phi}{dX^3}=0, \tag{23a}$$

$$\gamma_2\frac{d^2\Phi}{dX^2}-\gamma_1\frac{d^3W}{dX^3}-\gamma_3\Phi=0. \tag{23b}$$

The coefficients of Eq. (23) are defined as

$$P=\frac{\bar{P}L^2}{EI},k_s=\frac{\bar{k}_sL^2}{EI},k_L=\frac{\bar{k}_LL^4}{EI},k_{NL}=\frac{\bar{k}_{NL}L^6}{EI},\gamma_0=\frac{L^2}{S_0},$$
$$\gamma_1=\frac{4}{5},\gamma_2=\frac{68}{105},\gamma_3=\frac{8}{15}\frac{L^2}{S_0}\text{ and }S_0=\frac{I}{A}=\frac{1}{4}\left((R+t)^2+R^2\right). \tag{24}$$

The dimensionless boundary conditions can be written as

$$S-S:W=\frac{d^2W}{dX^2}=\frac{d\Phi}{dX}=0\text{at}X=0,1, \tag{25a}$$

$$C-C:W=\frac{dW}{dX}=\Phi=0\text{at}X=0,1. \tag{25b}$$

Since the definite integral in Eq. (23.a) can be treated as a constant term, Eq. (23) can be rewritten as

$$\frac{d^4W}{dX^4}+\Gamma^2\frac{d^2W}{dX^2}+k_LW+k_{NL}W^3-\gamma_1\frac{d^3\Phi}{dX^3}=0, \tag{26a}$$

$$\gamma_2\frac{d^2\Phi}{dX^2}-\gamma_1\frac{d^3W}{dX^3}-\gamma_3\Phi=0. \tag{26b}$$

In which

$$\Gamma^2=P-k_s-\frac{1}{2}\gamma_0\int_0^1\left(\frac{dW}{dX}\right)^2dx. \tag{26c}$$

The present model can be reduced to EBT by neglecting Eq. (26b) and substituting $\Phi=0$ into Eq. (26a).

3 Differential–integral–quadrature method (DIQM)

Owing to the presence of higher order nonlinearities, obtaining an analytical solution for the governing equations is too complicated. Therefore, numerical method is a suitable method to solve the buckling problem, Eq. (26). The DIQM presented in [31] is an efficient method to solve the nonlinear integro-differential equation.

In this method, the domain is discretized using the Chebyshev–Gauss–Lobatto as follows:

$$X_i=\frac{1}{2}\left(1-\cos\left(\frac{(i-1)\pi}{N-1}\right)\right),i=1,2,\dots N, \tag{27}$$

where N is the number of the grid points. On the basis of DQM, the r^{th}-order derivatives of $f(X)$ can be approximated as

$$\left.\frac{d^r f(X)}{dX^r}\right|_{X=X_i} = \sum_{j=1}^{N} \mathcal{M}_{ij}^{(r)} f\left(X_j\right), i = 1,2, \cdots N, \tag{28}$$

where $\mathcal{M}_{ij}^{(n)}$ is weighting coefficients of rth-order derivates. Quan and Chang (1989) introduced the weighting coefficients for the first-order derivative as

$$\mathcal{M}_{ij}^{(1)} = \begin{cases} \frac{\mathcal{L}^{(1)}(X_i)}{(X_i - X_j)\mathcal{L}^{(1)}(X_j)} i \neq j i, j = 1,2, \dots N \\ -\sum_{j=1, i\neq j}^{N} \mathcal{M}_{ij}^{(1)} i = j, i = 1,2, \dots N \end{cases}, \tag{29}$$

in which $\mathcal{L}^{(1)}(x)$ is defined as

$$\mathcal{L}^{(1)}(x) = \prod_{j=1, j\neq i}^{N} (X_i - X_j), \tag{30}$$

Introducing a column vector $\boldsymbol{f} = \left[f(X_i)\right] = \left[f_1, f_2, \dots f_N\right]^T$, in which $f(X_i)$ denotes the nodal value of $f(X)$ at $X = X_i$. Also, its first derivative vector will be $\boldsymbol{F} = \left[F_1, F_2, \dots F_N\right]^T$. A differential matrix of the first-order derivative based on Eq. (28) can be written in the form

$$\boldsymbol{F} = D^{(1)} \boldsymbol{f}. \tag{31}$$

Meanwhile, $D^{(1)} = \left[\mathcal{M}_{ij}^{(1)}\right], i, j = 1,2, \dots N$. The higher order derivative matrices can be obtained as

$$D^{(r)} = D^{(1)} D^{(r-1)}, r > 1, \tag{32}$$

Thereafter, an accurate row vector integral operator for definite integral is introduced. If we have a continuous function $f(x)$ in a domain $0 \leq X \leq 1$ and

$$\frac{df}{dX} = F(X), \tag{33}$$

then

$$\int_{X_i}^{X_j} F(X)dx = f\left(X_j\right) - f\left(X_i\right) \cong \sum_{k=1}^{N} \left([\mathcal{B}]_{jk} - [\mathcal{B}]_{ik}\right) F_k, \tag{34}$$

where $\mathcal{B}$ is the pseudo-inverse of matrix $D^{(1)}$. From Eq. (34), one can deduce that

$$\int_0^1 F(x)dx \cong \sum_{k=1}^{N} \left([\mathcal{B}]_{Nk} - [\mathcal{B}]_{1k}\right) F_k = \mathcal{R}\boldsymbol{F}. \tag{35}$$

Introducing a column vector $\boldsymbol{W}$ and $\boldsymbol{\Phi}$ as

$$\boldsymbol{W} = \left[W_1, W_2, \dots W_N\right]^T, \boldsymbol{\Phi} = \left[\Phi_1, \Phi_2, \dots \Phi_N\right]^T, \tag{36}$$

where $W_i = W\left(X_i\right)$ and $\Phi_i = \Phi\left(X_i\right)$. Upon using the DIQM, the nondimensional governing Eq. (26) can be discretized as follows:

$$\left(D^{(4)} + \Gamma^2 D^{(2)} + k_L I\right)\boldsymbol{W} + k_{NL} \boldsymbol{W}^{\circ 3} - \gamma_1 D^{(3)} \boldsymbol{\Phi} = 0, \tag{37a}$$

$$\left(\gamma_2 D^{(2)} - \gamma_3 I\right)\boldsymbol{\Phi} - \gamma_1 D^{(3)} \boldsymbol{W} = 0, \tag{37b}$$

$$\Gamma^2 - P + k_s + \frac{1}{2}\gamma_0 \mathcal{R}\left[\left(D^{(1)}\boldsymbol{W}\right)^{\circ 2}\right] = 0, \tag{37c}$$

in which I is $N \times N$ identity matrix and $\circ$ denotes the Hadamard matrix product. The discretized form of boundary conditions is

$$W_1 = W_N = \sum_{j=1}^{N} \left[D^{(2)} W\right]_{1j} = \sum_{j=1}^{N} \left[D^{(2)} W\right]_{Nj} = \sum_{j=1}^{N} \left[D^{(1)} \Phi\right]_{1j} = \sum_{j=1}^{N} \left[D^{(1)} \Phi\right]_{Nj} = 0, \tag{38a}$$

$$W_1 = W_N = \sum_{j=1}^{N} \left[D^{(1)} W\right]_{1j} = \sum_{j=1}^{N} \left[D^{(1)} W\right]_{Nj} = \Phi_1 = \Phi_N = 0. \tag{38b}$$

For S–S and C–C CNTs, respectively. Equation (37) forms a system of nonlinear algebraic equations which can be written in the form

$$\mathbb{T}\left(\mathcal{X}, \Gamma^2\right) = 0, \mathbb{T} : \mathbb{R}^{2N+1} \rightarrow \mathbb{R}^{2N+1}, \mathcal{X} = \left[\boldsymbol{W}^T, \boldsymbol{U}^T\right]^T. \tag{39}$$

Therefore, Eq. (39) can be solved by Newton's method. The Jacobian matrix of this system can be written as

$$\mathbb{J} = \begin{bmatrix} D^{(4)} + \Gamma^2 D^{(2)} + k_L I + 3k_{NL}\mathrm{diag}\left(\boldsymbol{W}^{\circ 2}\right) & \gamma_1 D^{(3)} & D^{(2)}\boldsymbol{W} \\ -\gamma_1 D^{(3)} & \left(\gamma_2 D^{(2)} - \gamma_3 I\right) & \boldsymbol{Z} \\ \gamma_0 \mathcal{R}\left(\left[\left(D^{(1)}\boldsymbol{W}\right)\boldsymbol{O}^T\right] \circ D^{(1)}\right) & \boldsymbol{Z}^T & 1 \end{bmatrix}, \tag{40}$$

where $\boldsymbol{Z}$ is a column vector defined as $\boldsymbol{Z}^T = [0, 0, \dots 0]_{N\times 1}$ and $\boldsymbol{O}$ is defined as $\boldsymbol{O}^T = [1,1, \dots 1]_{N\times 1}$. It is worth mentioning that, in Eqs. (39, 40), rows corresponding to boundaries are replaced by the corresponding boundary condition equations. Here, the solution of the linearized form of Eq. (39) is considered as the initial values to the Newton's method.

4 Analytical solutions

For the purpose of comparison, analytical solutions for post-buckling configuration and critical buckling load of S–S CNT are derived. The constants of elastic foundations are set to zeros (i.e., $k_L = k_s = k_{NL} = 0$). As consequence, Eq. (23) are reduced to

$$\frac{d^4W}{dX^4}+\left[P-\frac{1}{2}\gamma_0\int_0^1\left(\frac{dW}{dX}\right)^2dx\right]\frac{d^2W}{dX^2}-\gamma_1\frac{d^3\Phi}{dX^3}=0, \quad (41a)$$

$$\gamma_2\frac{d^2\Phi}{dX^2}-\gamma_1\frac{d^3W}{dX^3}-\gamma_3\Phi=0. \quad (41b)$$

According to Emam [17], the displacement field can be assumed as

$$W(X)=a\sin\left(\pi\frac{X}{L}\right), \quad (42a)$$

$$\Phi(X)=b\cos\left(\pi\frac{X}{L}\right), \quad (42b)$$

where a and b are unknowns to be determined. Substituting Eqs. (42.a, b) into Eqs. (41.a, b), the nondimensional maximum amplitude of post-buckling response of the first mode can be computed as

$$a=\pm\frac{2}{\pi\sqrt{\gamma_0}}\sqrt{P-\pi^2+\frac{\pi^2\gamma_1^2}{\gamma_3+\pi^2\gamma_2}}. \quad (43)$$

Also, the nondimensional first critical buckling load can be obtained as

$$\boldsymbol{P_c}=\pi^2\left(1-\frac{\pi^2\gamma_1^2}{\gamma_3+\pi^2\gamma_2}\right). \quad (44)$$

5 Numerical results

In this section, numerical results for the critical buckling load and the static response of zigzag and armchair SWCNTs with S–S and C–C boundary conditions are considered. The parameters used in the analysis for zigzag and armchair orientations of SWCNTs are the effective thickness is $t = 0.258$nm, the forces constants $K/2 = 46900\text{kcal/mol/nm}^2$, and $C/2 = 63\text{kcal/mol/rad}^2$.

5.1 Validation

To assure the accuracy of the present numerical method, the nondimensional critical buckling load and the post-buckling configuration of S–S zigzag and armchair SWCNTs without any elastic foundations are compared with analytical ones presented in Sect. 4. Table 1 compares the critical buckling loads of S–S zigzag and armchair SWCNTs obtained via DIQM with those obtained analytically, Eq. (44). As noticed, the DIQM and analytical results are in excellent agreement.

In Fig. 2, the post-buckling equilibrium paths of S–S zigzag and armchair SWCNTs based on the present method and analytical one, Eq. (43), are compared. Again, an excellent agreement is achieved.

5.2 Parametric studies

5.2.1 Effect of beam theories

The dimensionless first three buckling load of zigzag and armchair CNTs with various boundary conditions using different beam theories are reported in Tables 2 and 3, respectively. Here, the effect of surrounding medium is ignored. It is observed that, the critical buckling load predicted by HOSDT is smaller than those predicted by EBT. The difference between HOSDT and EBT is more pronounced for higher buckling modes and short CNTs. Increasing the CNT length, the results obtained by HOSDT converges to EBT.

Plotting in Fig. 3 are post-buckling equilibrium paths of (14, 0) zigzag CNT with S–S and C–C boundary conditions based on the HOSDT and EBT. Herein, the nondimensional post-buckling amplitude is defined as $\bar{W}=\frac{WL}{\sqrt{S_0}}$. It noted that the shear deformation has a great influence on the post-buckling response of CNT.

As noted from Tables 2, 3 and Fig. 3, the shear deformation effect can be neglected when the aspect ratio (L/D) reaches 50. Furthermore, it is observed that the shear deformation effect for C–C boundary conditions is more than S–S ones.

5.2.2 Effect of aspect ratio (L/D)

To study the effect of aspect ratio, the buckling load of zigzag and armchair CNTs with S–S and C–C boundary conditions are reported in Table 4. Herein, the elastic foundation constants are set to zeros. The (14, 0) zigzag

Table 1 Nondimensional first critical buckling load $\left(P_c=\frac{\bar{P}L^2}{EI}\right)$ of S–S zigzag and armchair CNT, ($k_L=k_s=k_{NL}=0$)

	L/D				
	5	10	20	50	100
(14, 0) zigzag CNT ($R = 5.4802$Å)					
Present	9.0253	9.6439	9.8122	9.8604	9.8673
Analytical	9.0253	9.6439	9.8122	9.8604	9.8673
(14, 14) armchair CNT ($R = 9.4920$Å)					
Present	9.1604	9.6821	9.8221	9.8620	9.8677
Analytical	9.1603	9.6821	9.8220	9.8620	9.8677

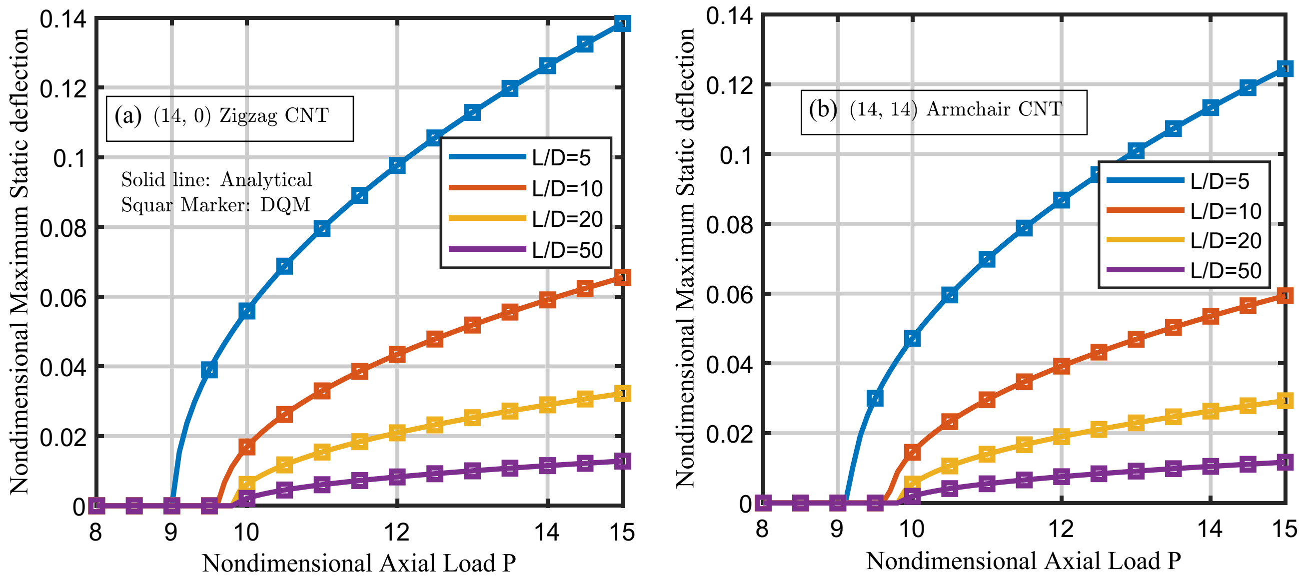

Fig. 2 Comparison of the post-buckling equilibrium paths of S–S zigzag and armchair CNT based on the DIQM and the analytical one, ($k_L = k_s = k_{NL} = 0$)

Table 2 Nondimensional first three critical buckling loads ($P_c = \frac{PL^2}{EI}$) of (14, 0) zigzag SWCNT ($R = 5.4802$Å)

B.Cs	Buckling mode	Beam theory	L/D				
			5	10	20	50	100
S–S	Mode 1	HOSDT	9.0253	9.6439	9.8122	9.8604	9.8673
		EBT	9.8696	9.8696	9.8696	9.8696	9.8696
	Mode 2	HOSDT	28.7540	36.1011	38.5755	39.3311	39.4415
		EBT	39.4784	39.4784	39.4784	39.4784	39.4784
	Mode 3	HOSDT	48.4186	73.3979	84.3837	88.0841	88.6397
		EBT	88.8264	88.8264	88.8264	88.8264	88.8264
C–C	Mode 1	HOSDT	28.754	36.101	38.5755	39.3311	39.4415
		EBT	39.4784	39.4784	39.4784	39.4784	39.4784
	Mode 2	HOSDT	44.1579	66.7652	76.7331	80.0923	80.5953
		EBT	80.7626	80.7626	80.7626	80.7626	80.7626
	Mode 3	HOSDT	53.8354	81.6987	144.4041	155.5827	157.3244
		EBT	157.9137	157.9137	157.9137	157.9137	157.9137

and (8, 8) armchair CNTs are considered so that they have approximately the same diameters that makes it possible to investigate the effect of chirality. As seen form Table 4, that armchair CNT relatively have a little higher values of critical buckling load compared to zigzag CNT especially for lower aspect ratios. In addition, one can note that, the buckling load of CNTs decreases rapidly as the aspect ratio increases. This can be interpreted since increasing aspect ratio decreases the CNT rigidity. The same conclusion can be drawn from Fig. 4 which contains plots of the critical buckling load versus aspect ratio of (8, 8) armchair S–S and C–C CNTs without any elastic foundations.

Figure 5 depicts the post-buckling equilibrium path of (8, 8) armchair S–S and C–C CNTs with different values of aspect ratio. It can be seen that increasing aspect ratio causes the CNTs to behave softer and consequently the maximum deflection to increase.

5.2.3 Effect of elastic foundation constants

In Table 5, the influence of elastic foundation constants on the critical buckling loads of S–S and C–C CNTs with aspect ratio $L/D = 10$ are studied. Different types of CNTs are considered. Table 5 reveals that the critical buckling load increases by increasing shear and linear elastic foundation parameters. However, the nonlinear elastic foundation parameter has no effect on the critical buckling load. It can easily be seen from Eq. (37.a) and the Jacobian

Table 3 Nondimensional first three critical buckling loads $\left(P_c = \frac{\bar{P}L^2}{EI}\right)$ of (14,14) armchair CNT ($R = 9.4920$Å)

B.Cs	Buckling mode	Beam theory	L/D 5	10	20	50	100
S–S	Mode 1	HOSDT	9.1604	9.6821	9.8221	9.8620	9.8677
		EBT	9.8696	9.8696	9.8696	9.8696	9.8696
	Mode 2	HOSDT	30.1624	36.6414	38.7283	39.3565	39.4479
		EBT	39.4784	39.4784	39.4784	39.4784	39.4784
	Mode 3	HOSDT	52.5053	75.6604	85.1178	88.2113	88.6719
		EBT	88.8264	88.8264	88.8264	88.8264	88.8264
C–C	Mode 1	HOSDT	30.1624	36.6414	38.7283	39.3565	39.4479
		EBT	39.4784	39.4784	39.4784	39.4784	39.4784
	Mode 2	HOSDT	47.8497	68.817	77.3996	80.2076	80.6243
		EBT	80.7626	80.7626	80.7626	80.7626	80.7626
	Mode 3	HOSDT	56.5765	88.1514	146.5653	155.9798	157.4257
		EBT	157.9137	157.9137	157.9137	157.9137	157.9137

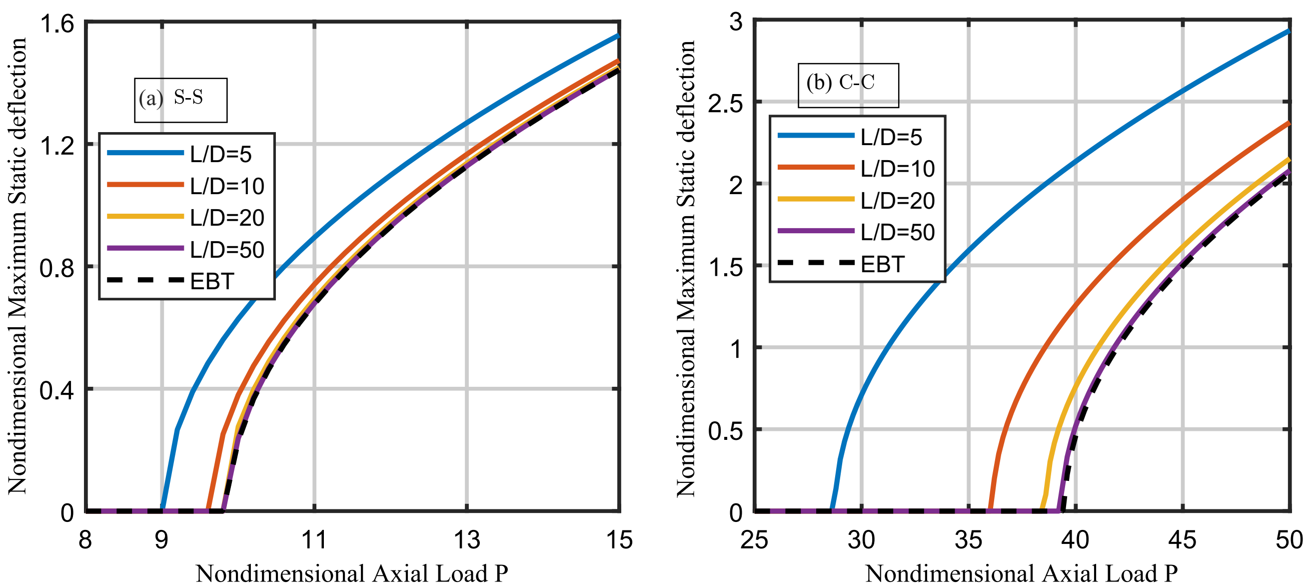

Fig. 3 Post-buckling equilibrium paths of S–S and C–C (14, 0) zigzag CNT obtained by HOSDT and EBT, ($k_L = k_s = k_{NL} = 0$)

Table 4 First critical buckling load (nN) of S–S and C–C zigzag and armchair CNTs, ($k_L = k_s = k_{NL} = 0$)

B.Cs	L/D 5	10	20	50
(14, 0) zigzag CNT ($R = 5.4802$Å)				
S–S	81.81860	21.85663	5.55951	0.89389
C–C	260.66858	81.81838	21.85657	3.56555
(8, 8) armchair CNT ($R = 5.4240$Å)				
S–S	82.07582	21.93157	5.57904	0.89705
C–C	261.26835	82.07536	21.93151	3.57809

matrix Eq. (40), that the nonlinear elastic foundation parameter k_{NL} is multiplied by the static response $\boldsymbol{W}$. In fact, the static response of CNTs in prebuckling state is zero, as shown in Fig. 3. And hence, the nonlinear elastic foundation parameter has no effect on the buckling load of CNTs. Also, it can be noted that the influence of the shear and linear elastic foundation parameters on critical buckling load become more considerable as the chiral number of CNTs increases. Furthermore, it can be observed that the chiral number has a significant effect on the critical

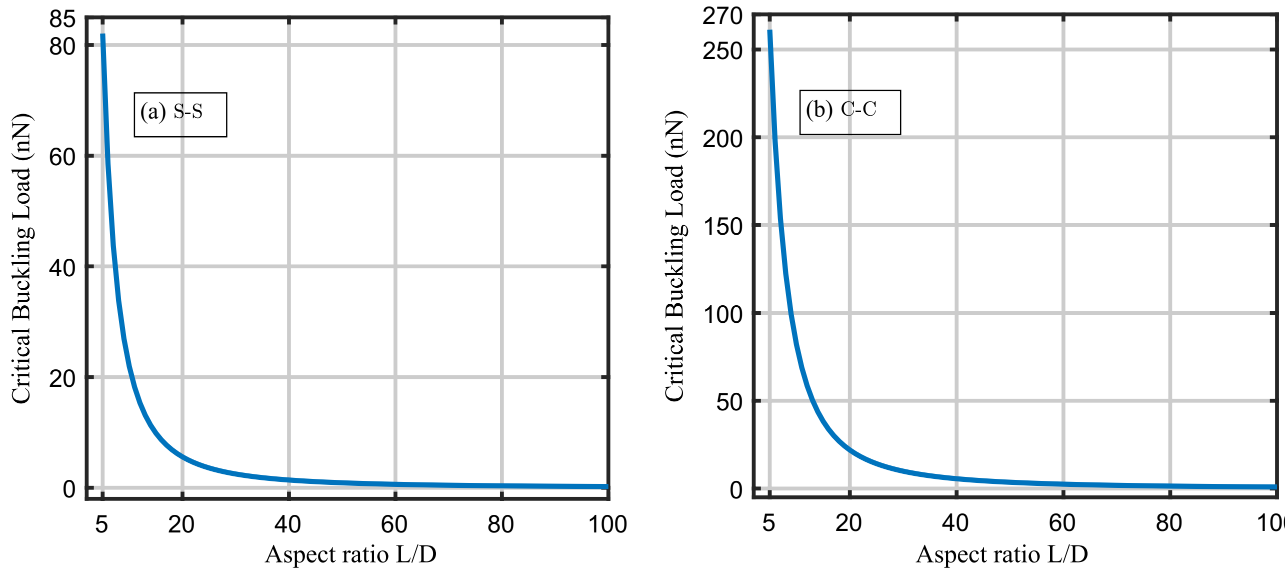

Fig. 4 Critical buckling load versus aspect ratio of (8, 8) armchair S–S and C–C CNTs, ($k_L = k_s = k_{NL} = 0$)

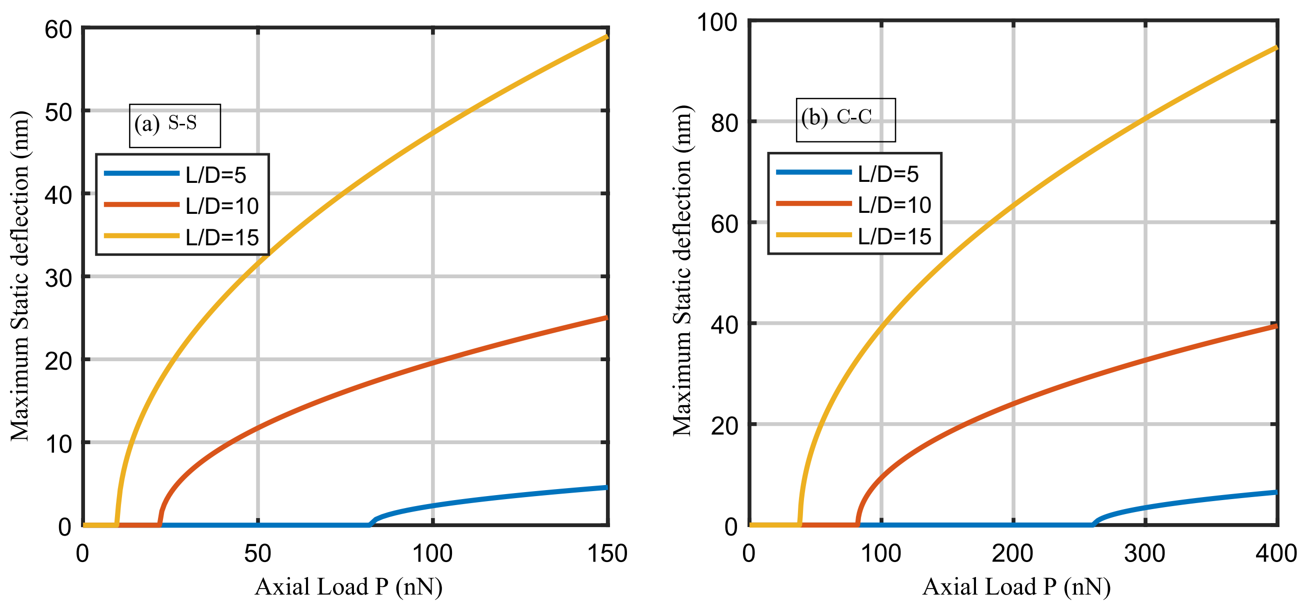

Fig. 5 Post-buckling equilibrium paths of S–S and C–C (8, 8) armchair CNTs with different values of aspect ratio, ($k_L = k_s = k_{NL} = 0$)

buckling load of CNTs. These observations are valid for both zigzag and armchair CNTs.

Figure 6 illustrates post-buckling equilibrium paths of S–S and C–C (7, 7) armchair CNTs with various values of elastic foundation constants and aspect ratio $L/D = 10$. It can be easily deduced that the responses have a descending trend with respect to the shear foundation constant. The shear stiffness of elastic foundation is more significant than that of the linear and nonlinear elastic foundation constants.

Table 5 First critical buckling load (nN) of different types of CNT with S–S and C–C boundary conditions ($L/D = 10$)

B. Cs	CNT type	k_L	$k_{NL} = 0$			$k_{NL} = 10$		
			$k_s = 0$	5	10	$k_s = 0$	5	10
S–S	(7, 0) zigzag $R = 2.7401$Å	0	18.58863	28.33804	38.08746	18.58863	28.33804	38.08746
		25	23.52768	33.27710	43.02652	23.52768	33.27710	43.02652
		50	28.46693	38.21635	47.96576	28.46693	38.21635	47.96576
	(14, 0) zigzag $R = 5.4802$Å	0	21.85663	33.18847	44.52031	21.85663	33.18847	44.52031
		25	27.59734	38.92918	50.26102	27.59734	38.92918	50.26102
		50	33.33827	44.67011	56.00195	33.33827	44.67011	56.00195
	(7, 7) armchair $R = 4.7460$Å	0	20.91027	31.76868	42.62710	20.91027	31.76868	42.62710
		25	26.41136	37.26977	48.12819	26.41136	37.26977	48.12819
		50	31.91223	42.77065	53.62906	31.91223	42.77065	53.62906
	(14, 14) armchair $R = 9.4920$Å	0	29.28060	44.40160	59.52259	29.28060	44.40160	59.52259
		25	36.94090	52.06189	67.18289	36.94090	52.06189	67.18289
		50	44.60150	59.72249	74.84349	44.60150	59.72249	74.84349
C–C	(7, 0) zigzag $R = 2.7401$Å	0	67.46655	77.21596	86.96538	67.46655	77.21596	86.96538
		25	71.15261	80.90202	90.65144	71.15261	80.90202	90.65144
		50	74.80064	84.55006	94.29948	74.80064	84.55006	94.29948
	(14, 0) zigzag $R = 5.4802$Å	0	81.81838	93.15022	104.48206	81.81838	93.15022	104.48206
		25	86.10680	97.43864	108.77048	86.10680	97.43864	108.77048
		50	90.35986	101.69170	113.02354	90.35986	101.69170	113.02354
	(7, 7) armchair $R = 4.7460$Å	0	77.93779	88.79621	99.65463	77.93779	88.79621	99.65463
		25	82.04662	92.90503	103.76345	82.04662	92.90503	103.76345
		50	86.12026	96.97868	107.83709	86.12026	96.97868	107.83709
	(14, 14) armchair $R = 9.4920$Å	0	110.81090	125.93190	141.05289	110.81090	125.93190	141.05289
		25	116.53510	131.65610	146.77710	116.53510	131.65610	146.77710
		50	122.21576	137.33676	152.45775	122.21576	137.33676	152.45775

6 Conclusions

In the framework of higher order beam theory, buckling and post-buckling behaviors of zigzag and armchair CNTs resting on nonlinear elastic medium were numerically investigated. S–S and C–C boundary conditions are considered. The nonlinear integro-differential equations were solved by DIQM method in combination with Newton method. Also, they are solved analytically for the case of S–S boundary conditions. Results obtained via DIQM method were compared with those obtained by analytical solutions and an excellent agreement was obtained. The most findings of the current analysis are

- The critical buckling load predicted by HOSDT is smaller than those predicted by EBT.
- The difference between HOSDT and EBT is more pronounced for higher buckling modes and short CNTs.
- The armchair CNT relatively have a little higher values of critical buckling load compared to zigzag CNT especially for lower aspect ratios.
- The buckling load of CNTs decreases rapidly as the aspect ratio increases. This can be interpreted since increasing aspect ratio decreases the CNT rigidity.
- The critical buckling load increases by increasing shear and linear elastic foundation parameters. However, the nonlinear elastic foundation parameter has no effect on the critical buckling load.

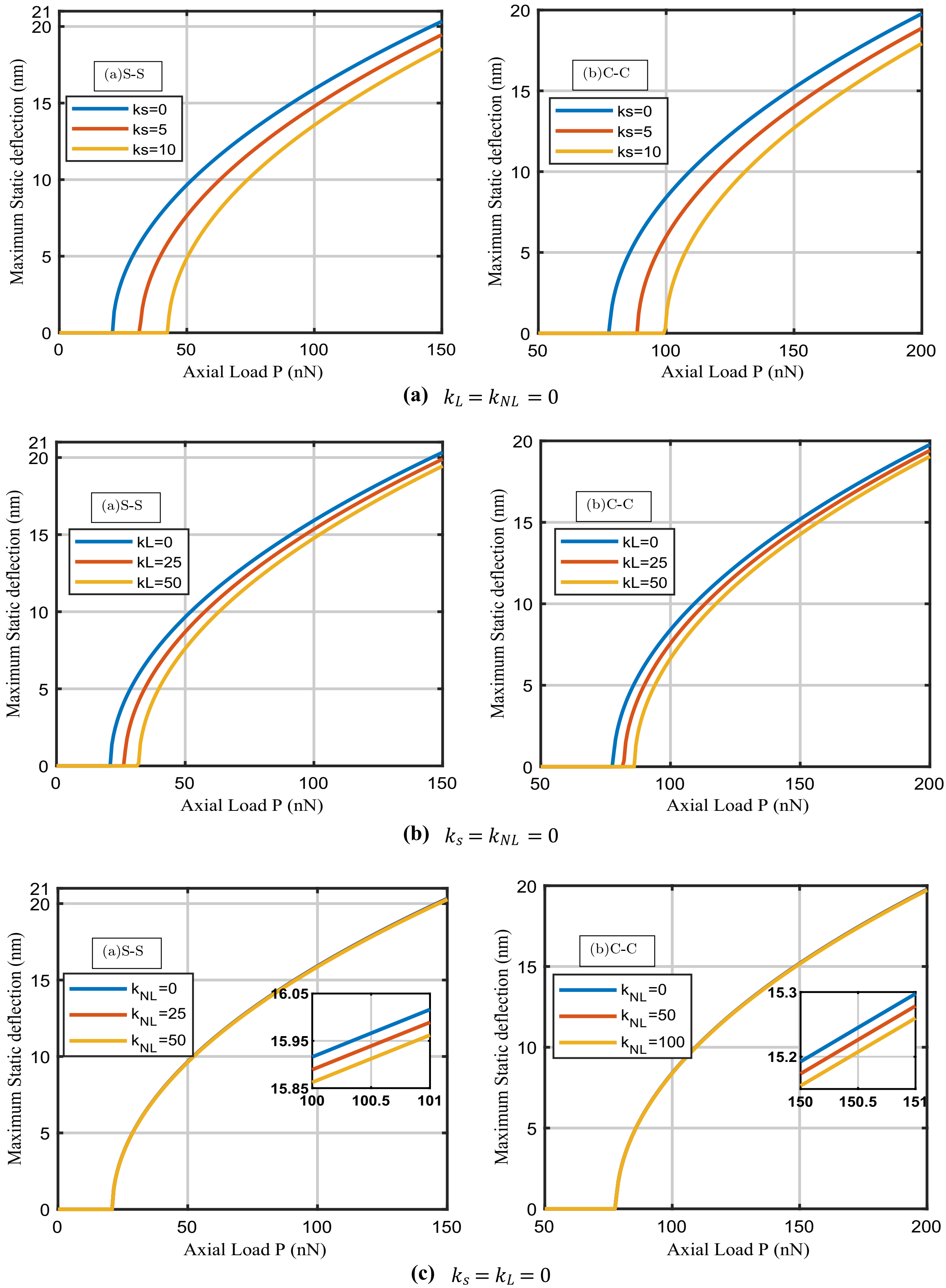

Fig. 6 Post-buckling equilibrium paths of S–S and C–C (7, 7) armchair CNTs with aspect ratio $L/D = 10$

Acknowledgements This work was funded by the Deanship of Scientific Research (DSR), King Abdulaziz University, Jeddah, under Grant No. (D-423-135-1441). The authors, therefore, acknowledge with thanks DSR technical and financial support.

References

1. Aydogdu M (2008) Vibration of multi-walled carbon nanotubes by generalized shear deformation theory. Int J Mech Sci 50(4):837–844
2. Baghdadi H, Tounsi A, Zidour M, Benzair A (2014) Thermal effect on vibration characteristics of armchair and zigzag single-walled carbon nanotubes using nonlocal parabolic beam theory. Fuller Nanotub Carbon Nanostruct 23(3):266–272
3. Bedia WA, Benzair A, Semmah A, Tounsi A, Mahmoud SR (2015) On the thermal buckling characteristics of armchair single-walled carbon nanotube embedded in an elastic medium based on nonlocal continuum elasticity. Braz J Phys 45(2):225–233
4. Benguediab S, Tounsi A, Zidour M, Semmah A (2014) Chirality and scale effects on mechanical buckling properties of zigzag double-walled carbon nanotubes. Compos B Eng 57:21–24
5. Besseghier A, Heireche H, Bousahla AA, Tounsi A, Benzair A (2015) Nonlinear vibration properties of a zigzag single-walled carbon nanotube embedded in a polymer matrix. Adv Nano Res 3(1):029
6. Dehghan M, Ebrahimi F, Vinyas M (2019) Wave dispersion characteristics of fluid-conveying magneto-electro-elastic nanotubes. Eng Comput. https://doi.org/10.1007/s00366-019-00790-5
7. Ebrahimi F, Hosseini SHS (2019) Nonlinear vibration and dynamic instability analysis nanobeams under thermo-magneto-mechanical loads: a parametric excitation study. Eng Comput. https://doi.org/10.1007/s00366-019-00830-0
8. Ebrahimi F, Karimiasl M, Mahesh V (2019) Chaotic dynamics and forced harmonic vibration analysis of magneto-electro-viscoelastic multiscale composite nanobeam. Eng Comput. https://doi.org/10.1007/s00366-019-00865-3
9. Eltaher MA, Agwa MA (2016) Analysis of size-dependent mechanical properties of CNTs mass sensor using energy equivalent model. Sens Actuators A 246:9–17
10. Eltaher MA, El-Borgi S, Reddy JN (2016) Nonlinear analysis of size-dependent and material-dependent nonlocal CNTs. Compos Struct 153:902–913
11. Eltaher MA, Agwa M, Kabeel A (2018) Vibration analysis of material size-dependent CNTs using energy equivalent model. J Appl Comput Mech 4(2):75–86
12. Eltaher MA, Mohamed N, Mohamed S, Seddek LF (2019a) Postbuckling of curved carbon nanotubes using energy equivalent model. J Nano Res 57:136–157 **(Trans Tech Publications)**
13. Eltaher MA, Mohamed N, Mohamed SA, Seddek LF (2019) Periodic and nonperiodic modes of postbuckling and nonlinear vibration of beams attached to nonlinear foundations. Appl Math Model 75:414–445
14. Eltaher MA, Almalki TA, Ahmed KI, Almitani KH (2019) Characterization and behaviors of single walled carbon nanotube by equivalent-continuum mechanics approach. Adv Nano Res 7(1):39–49
15. Eltaher MA, Almalki TA, Almitani KH, Ahmed KIE (2019) Participation factor and vibration of carbon nanotube with vacancies. J Nano Res 57:158–174 **(Trans Tech Publications)**
16. Eltaher MA, Almalki TA, Almitani KH, Ahmed KIE, Abdraboh AM (2019) Modal participation of fixed–fixed single-walled carbon nanotube with vacancies. Int J Adv Struct Eng 11(2):151–163
17. Emam SAJCS (2011) Analysis of shear-deformable composite beams in postbuckling. Compos Struct 94(1):24–30
18. Emam SA, Eltaher MA, Khater ME, Abdalla WS (2018) Postbuckling and free vibration of multilayer imperfect nanobeams under a pre-stress load. Appl Sci 8(11):2238
19. Ghadyani G, Öchsner A (2015) On a thickness free expression for the stiffness of carbon nanotubes. Solid State Commun 209:38–44
20. Gholami R, Ansari R, Gholami Y (2017) Nonlinear resonant dynamics of geometrically imperfect higher-order shear deformable functionally graded carbon-nanotube reinforced composite beams. Compos Struct 174:45–58
21. Heshmati M, Yas MH, Daneshmand F (2015) A comprehensive study on the vibrational behavior of CNT-reinforced composite beams. Compos Struct 125:434–448
22. Iijima S (1991) Helical microtubules of graphitic carbon. Nature 354(6348):56–58
23. Joshi UA, Sharma SC, Harsha SP (2012) A multiscale approach for estimating the chirality effects in carbon nanotube reinforced composites. Phys E 45:28–35
24. Karimiasl M, Ebrahimi F, Mahesh V (2019) Postbuckling analysis of piezoelectric multiscale sandwich composite doubly curved porous shallow shells via Homotopy Perturbation Method. Eng Comput. https://doi.org/10.1007/s00366-019-00841-x
25. Khater ME, Eltaher MA, Abdel-Rahman E, Yavuz M (2014) Surface and thermal load effects on the buckling of curved nanowires. Eng Sci Technol Int J 17(4):279–283
26. Kordkheili SAH, Mousavi T, Bahai H (2018) Nonlinear dynamic analysis of SWNTs conveying fluid using nonlocal continuum theory. Struct Eng Mech 66(5):621–629
27. Leung AYT, Guo X, He XQ, Kitipornchai S (2005) A continuum model for zigzag single-walled carbon nanotubes. Appl Phys Lett 86(8):083110
28. Maneshi MA, Ghavanloo E, Fazelzadeh SA (2018) Closed-form expression for geometrically nonlinear large deformation of nanobeams subjected to end force. Eur Phys J Plus 133(7):256
29. Mayoof FN, Hawwa MA (2009) Chaotic behavior of a curved carbon nanotube under harmonic excitation. Chaos Solitons Fractals 42(3):1860–1867
30. Mikata Y (2007) Complete solution of elastica for a clamped-hinged beam, and its applications to a carbon nanotube. Acta Mech 190(1–4):133–150
31. Mohamed N, Eltaher MA, Mohamed SA, Seddek LF (2018) Numerical analysis of nonlinear free and forced vibrations of buckled curved beams resting on nonlinear elastic foundations. Int J Non-Linear Mech 101:157–173
32. Mohamed N, Eltaher MA, Mohamed SA, Seddek LF (2019) Energy equivalent model in analysis of postbuckling of imperfect carbon nanotubes resting on nonlinear elastic foundation. Struct Eng Mech 70(6):737–750
33. Mohammadi H, Mahzoon M, Mohammadi M, Mohammadi M (2014) Postbuckling instability of nonlinear nanobeam with geometric imperfection embedded in elastic foundation. Nonlinear Dyn 76(4):2005–2016
34. Nasdala L, Kempe A, Rolfes R (2012) Are finite elements appropriate for use in molecular dynamic simulations? Compos Sci Technol 72(9):989–1000
35. Rappé AK, Casewit CJ, Colwell KS, Goddard Iii WA, Skiff WM (1992) UFF, a full periodic table force field for molecular mechanics and molecular dynamics simulations. J Am Chem Soc 114(25):10024–10035
36. Reddy JN (1984) A simple higher-order theory for laminated composite plates. J Appl Mech 51(4):745–752
37. She GL, Yuan FG, Ren YR (2017) Thermal buckling and post-buckling analysis of functionally graded beams based on a general higher-order shear deformation theory. Appl Math Model 47:340–357
38. Shodja HM, Delfani MR (2011) A novel nonlinear constitutive relation for graphene and its consequence for developing

closed-form expressions for Young's modulus and critical buckling strain of single-walled carbon nanotubes. Acta Mech 222(1–2):91–101

39. Shokrieh MM, Rafiee R (2010) Prediction of Young's modulus of graphene sheets and carbon nanotubes using nanoscale continuum mechanics approach. Mater Des 31(2):790–795
40. Wang B, Deng Z, Zhang K, Zhou J (2012) Dynamic analysis of embedded curved double-walled carbon nanotubes based on nonlocal Euler-Bernoulli Beam theory. Multidiscip Model Mater Struct 8(4):432–453
41. Wang B, Deng ZC, Zhang K (2013) Nonlinear vibration of embedded single-walled carbon nanotube with geometrical imperfection under harmonic load based on nonlocal Timoshenko beam theory. Appl Math Mech 34:269–280
42. Wu Y, Zhang X, Leung AYT, Zhong W (2006) An energy-equivalent model on studying the mechanical properties of single-walled carbon nanotubes. Thin-Walled Struct 44(6):667–676